Ferromagnetism, variable range hopping, and the anomalous Hall effect in epitaxial Co:ZnO thin film*

Bai Hong-Liang(白洪亮), He Shu-Min(贺树敏), Xu Tong-Shuai(徐同帅), Liu Guo-Lei(刘国磊)†, Yan Shi-Shen(颜世申), Zhu Da-Peng(朱大鹏), Dai Zheng-Kun(代正坤), Yang Feng-Fan(杨丰帆), Dai You-Yong(代由勇), Chen Yan-Xue(陈延学), and Mei Liang-Mo(梅良模)

School of Physics and National Key Laboratory of Crystal Materials, Shandong University, Jinan 250100*, China*

(Received 9 February 2012; revised manuscript received 1 April 2012)

A series of high quality single crystalline epitaxial $Zn_{0.95}Co_{0.05}O$ thin films is prepared by molecular beam epitaxy. Superparamagnetism and ferromagnetism are observed when the donor density is manipulated in a range of 10^{18} cm^{-3}–10^{20} cm^{-3} by changing the oxygen partial pressure during film growth. The conduction shows variable range hopping at low temperature and thermal activation conduction at high temperature. The ferromagnetism can be maintained up to room temperature. However, the anomalous Hall effect is observed only at low temperature and disappears above 160 K. This phenomenon can be attributed to the local ferromagnetism and the decreased optimal hopping distance at high temperatures.

Keywords: ZnCoO, variable range hopping, anomalous Hall effect

PACS: 72.20.–i, 72.25.Dc **DOI:** 10.1088/1674-1056/21/10/107201

1. Introduction

The

Co-doped ZnO magnetic semiconductor has attracted intensive attention due to its potential applications in spintronic devices.[1−3] Varied magnetisms were observed, such as room temperature ferromagnetism, paramagnetism, spin-glass, and antiferromagnetism.[4−10] Many models were proposed to understand the origin of ferromagnetism, such as double exchange, carrier-mediated exchange,[11] and bound magnetic polaron models.[12] Experimental results[13,14] showed that room temperature ferromagnetism is easily observed in defect abundant samples, and theoretical calculations[15,16] showed that defects play a crucial role in the ferromagnetic coupling between Co atoms. As is well known, the native defects in ZnO, such as zinc interstitials and oxygen vacancies,[17−19] greatly affect the electronic transport. Anomalous Hall effect (AHE)[20] is a direct tool to detect the spin-polarized current. For ZnCoO with low Co doping, AHE was usually observed at low temperature.[5,10] Up to now, the existence of spin-polarized current for ZnCoO at a practical temperature is still dubious. Moreover, because of the multiple mechanisms of electronic transport,[21−23] the correlation between ferromagnetism and magnetic transport has not yet been established. In this work, we investigate the magnetism and spin correlated electronic transport by using high-quality $Zn_{1-x}Co_xO$ films prepared by molecular beam epitaxy. It may give an indication of obtaining spin-polarized current in a wide temperature range.

2. Experiment

Co-doped ZnO thin films were grown on commercial *c*-plane $Al_2O_3(0001)$ substrates by oxygen plasma assisted molecular beam epitaxy. Co and Zn fluxes were co-evaporated from high-purity Co and Zn solid sources in *k*-cells. An Oxford scientific radio frequency plasma source was used to provide a reactive oxygen plasma. The flux ratio of Co/Zn was manipulated by a quartz microbalance. The $Zn_{1-x}Co_xO$ thin films were grown on a 50-nm ZnO buffer layer at a relatively low temperature 420 °C to achieve high Co doping without destroying the crystal quality too much. The normal growth rate was about 2.5 nm per minute. The Co concentration was designed to be

*Project supported by the State Key Project of Fundamental Research of China (Grant No. 2009CB929202) and the National Natural Science Foundation of China (Grant Nos. 10834001 and 51125004).

†Corresponding author. E-mail: liu-guolei@sdu.edu.cn

© 2012 Chinese Physical Society and IOP Publishing Ltd

$\sim$ 5% which was cross-checked by *in situ* X-ray photoelectron spectroscopy and *ex situ* energy dispersive X-ray analysis. The oxygen partial pressure was varied in a range of 3×10^{-5} Pa–2×10^{-3} Pa in which the doping film can keep a high-quality single crystalline structure. The surface structure was monitored by the real time reflection high energy electron diffraction system (RHEED). The crystal structure was characterized by high resolution X-ray diffraction (HRXRD, Bruker D5005HR). The electric transport properties were measured by the Quantum Designed Superconductivity Quantum Interference Device (SQUID) system, and the magnetic properties were characterized by SQUID and an alternative gradient magnetometer (AGM). The thicknesses of $Zn_{0.95}Co_{0.05}O$ thin films used in this paper are 300 nm–500 nm.

3. Results and discussion

Figure 1(a) shows the saturation magnetization (M_S) of a series of $Zn_{0.95}Co_{0.05}O$ films prepared under different values of oxygen partial pressure (P_O) in a range of 3×10^{-5} Pa– 2×10^{-3} Pa. The magnetic field is applied in the direction perpendicular to the film surface, and the paramagnetic and diamagnetic backgrounds are subtracted linearly. According to the behaviours of magnetism and electric transport, $Zn_{0.95}Co_{0.05}O$ films can be classified into three regions which are separated by dashed lines in Fig. 1(a). In the left low P_O region with $P_O < 1.7\times10^{-3}$ Pa, $Zn_{0.95}Co_{0.05}O$ film presents robust ferromagnetism at room temperature and its M_S increases abruptly with P_O reducing. When $P_O < 2\times10^{-5}$ Pa, single crystalline $Zn_{0.95}Co_{0.05}O$ films are difficult to obtain because of oxygen deficiency. These polycrystalline samples may have complicated phases and/or defects, and they are not considered in the paper. In the middle region in Fig. 1(a), $Zn_{0.95}Co_{0.05}O$ film also presents room temperature ferromagnetism with smaller M_S. In the right region with $P_O > 5\times10^{-4}$ Pa, only superparamagnetism is observed.

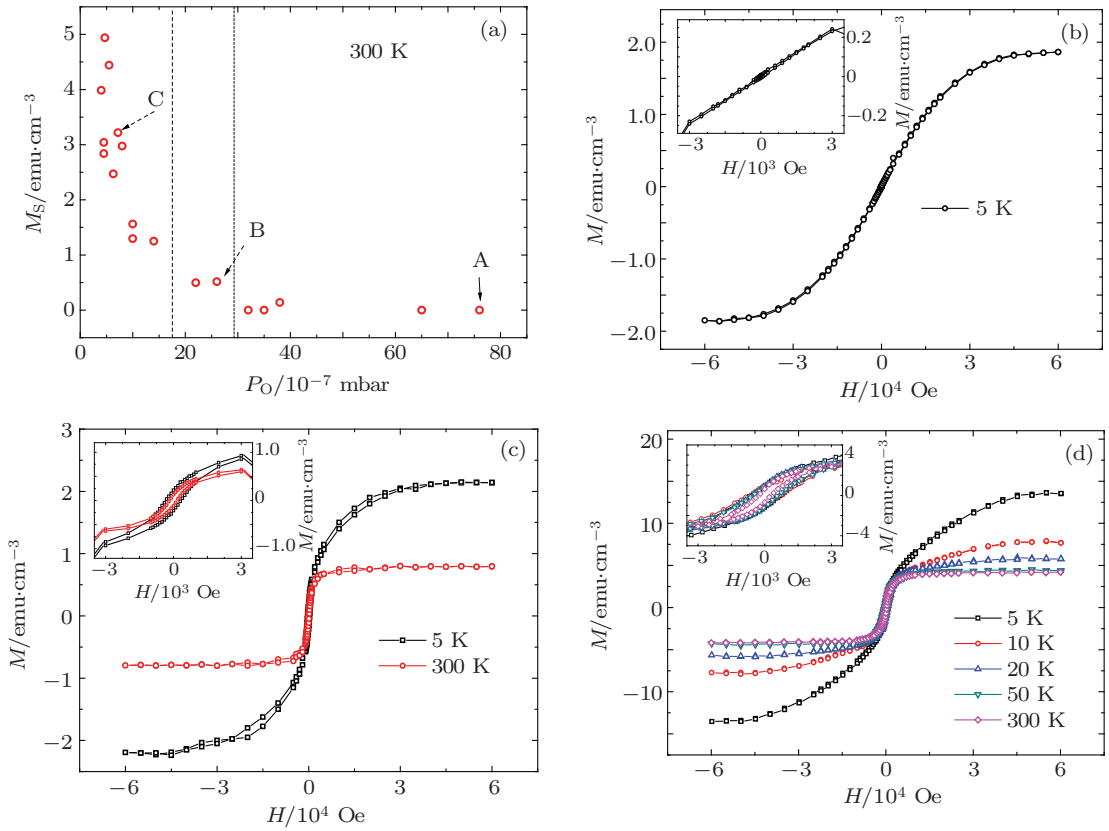


Fig. 1. (colour online) (a) Dependences of saturation magnetization M_S on P_O for a series of $Zn_{0.95}Co_{0.05}O$ thin films measured by AGM, the marked samples A, B, and C are selected as three typical samples. M–H hysteresis loops measured by SQUID for (b) sample A at 5 K, (c) sample B at 5 K and 300 K, and (d) sample C between 5 K and 300 K. The insets in panels (b)–(d) show the zoom-in M–H loops at low field. The applied magnetic field is perpendicular to the surface. The paramagnetic and diamagnetic background signals are subtracted linearly. 1 bar=10^5 Pa, 1 Oe=79.5775 A/m.

Figures 1(b)–1(d) show the magnetization curves of three typical samples named samples A, B, and C coming from three different regions. Sample A shows superparamagnetism at 5 K. Obvious hysteresis loops are observed in samples B and C, each of which presents robust ferromagnetism at room temperature. Moreover, sample C has an average magnetic moment of 0.22 μ_B per Co^{2+} ion at room temperature and a large coercive field of 280 Oe (1 Oe=79.5775 A/m), while sample B has a much smaller moment and coercive field 170 Oe.

Figures 2(a)–2(c) show the HRXRD θ–2θ scans, and corresponding RHEED patterns and rocking curves for samples A, B, and C, respectively. The HRXRD results indicate that ZnCoO films each have a wurtzite ZnO structure and no secondary phases are observed. With P_O decreasing, the RHEED pattern becomes streaky dots due to the oxygen deficiency. The rocking curves at ZnCoO(0002) peak show that the full widths at half maximum (FWHMs) are 0.32°, 0.38°, and 0.55° for samples A, B, and C, respectively, which indicates that each of the ZnCoO films has a high-quality single crystal structure, and the lower P_O only slightly reduces the crystallization.

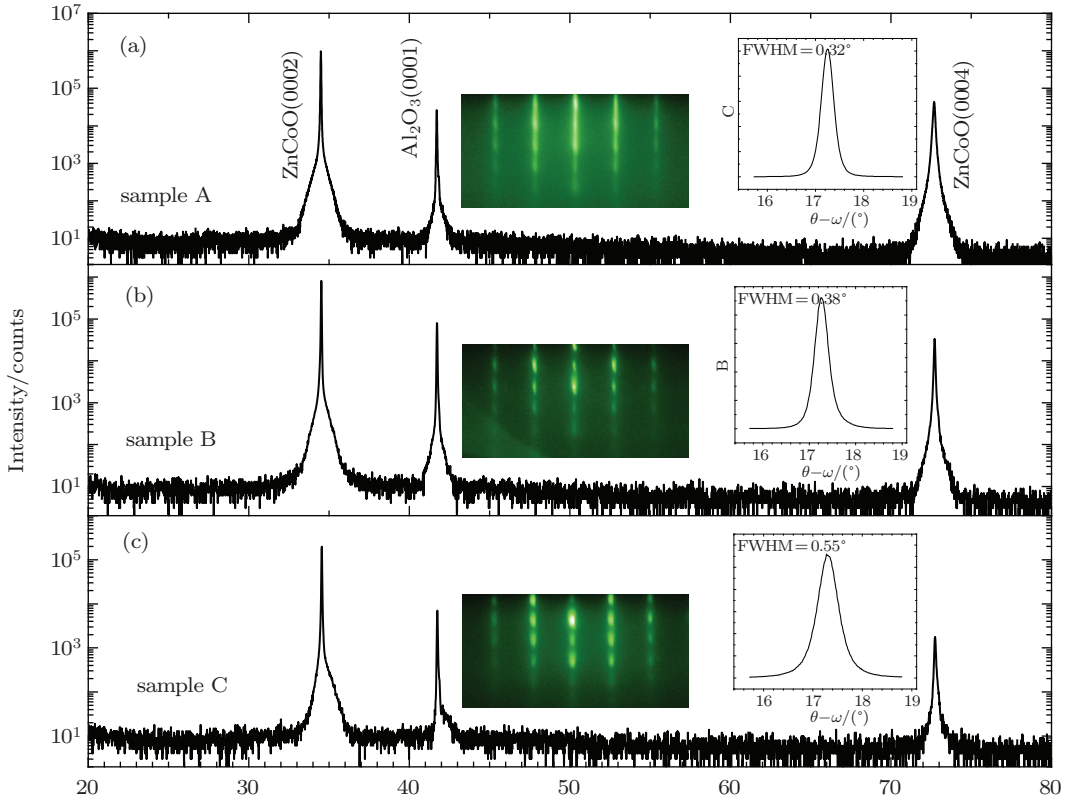


Fig. 2. (colour online) (a)–(c) XRD θ–2θ scanning curves of $Zn_{0.95}Co_{0.05}O$ thin films for samples A, B, and C. The insets show the corresponding RHEED patterns with electron beam azimuths along $[11\text{-}20]_{ZnO}$ and rocking curves at ZnCoO(0002) peak.

The sheet resistivity ρ (or conductivity σ) is measured in four-point van der Pauw geometry. Figure 3(a) shows that the values of ρ for all samples A, B, and C decrease monotonically with temperature T increasing, indicating typical semiconductor behaviours. The conductivity can be well fitted using a phenomenological model as shown in Figs. 3(b)–3(d). Generally, the conductivity σ includes two parts: conduction from variable range hopping (VRH) at low temperature, and thermal activation conduction at high temperature.

The conductivity of sample A can be written as the sum of Efros VRH conduction[24] and thermal activation conduction, i.e.,

$$\sigma = A\exp\left[-\left(\frac{T_{ES}}{T}\right)^{1/2}\right] + \sigma_{th0}\exp\left[-\frac{E_d}{2k_BT}\right], \quad (1)$$

where k_B is the Boltzmann's constant, A and T_{ES} are the prefactor and characteristic temperature for the Efros VRH, σ_{th0} and E_d are the prefactor and activa-

tion energy (energy gap between localized donor states and the bottom of conduction band) for thermal activation conductivity, respectively. A linear relationship between $\ln\sigma$ and $T^{-1/2}$ at low temperatures indicates the Efros VRH conduction as shown in the inset of Fig. 3(b). The Efros VRH means that the long rang Coulomb interaction between charge carriers plays a role in the electrical transport.

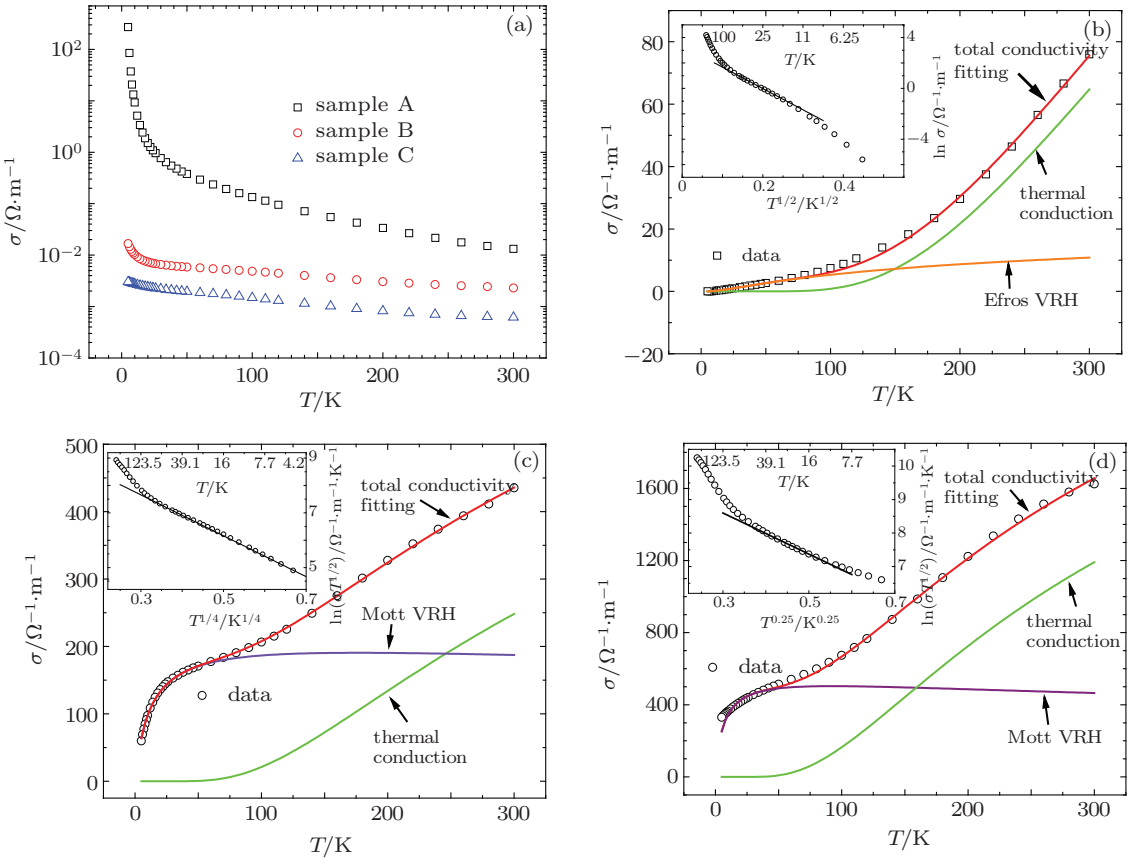


Fig. 3. (colour online) (a) Temperature-dependent sheet resistivities for samples A, B, and C. Fitting plots of longitudinal conductivity $\sigma(T)$, (b) for sample A with Eq. (1) (the inset shows $\ln\sigma$–$T^{-1/2}$), (c) for sample B with Eq. (2) (the inset shows $\ln(\sigma T^{1/2})$–$T^{-1/4}$), and (d) for sample C with Eq. (2) (the inset shows $\ln(\sigma T^{1/2})$–$T^{-1/4}$).

The resulting conductivity σ of sample B can be written as the sum of Mott VRH conduction[25] and thermal activation conduction, i.e.,

$$\sigma = BT^{-1/2}\exp\left[-\left(\frac{T_{\rm M}}{T}\right)^{1/4}\right] + \sigma_{\rm th0}\exp\left[-\frac{E_{\rm d}}{2k_{\rm B}T}\right], \quad (2)$$

where $BT^{-1/2} = \sigma_{\rm M0}$. In a temperature range between 5 K and 100 K, $\ln(\sigma T^{1/2})$ depends linearly on $T^{-1/4}$, which can be attributed to typical Mott VRH[25] as shown in the inset of Fig. 3(c). The Mott VRH conductivity can be written as

$$\sigma_{\rm M} = \sigma_{\rm M0}\exp[-(T_{\rm M}/T)^{1/4}]$$

with

$$\sigma_{\rm M0} = e^2\nu_{\rm ph}[N(E_{\rm F})/(32\pi\alpha k_{\rm B}T)]^{1/2}$$

and $T_{\rm M} = 18.1\alpha^3/(k_{\rm B}N(E_{\rm F}))$. Here $\nu_{\rm ph}$ is the highest phonon frequency (1.7×10^{13} Hz for ZnO crystal), $N(E_{\rm F})$ is the density of localized electronic states at Fermi level $E_{\rm F}$, and α is the inverse of localization length ξ. The optimal hopping distance can be calculated as

$$R_{\rm M} = [9/(8\pi\alpha N(E_{\rm F})k_{\rm B}T)]^{1/4}. \quad (3)$$

Figure 3(d) shows that the conductivity of sample C can also be fitted using the same phenomenological model as that for sample B, though its sheet conductivity is much larger than that of sample B. The slight deviation of the fitting curve from experimental data below 10 K is caused by the increased nearest neighbour hopping (NNH) due to the increased donors. The obtained physical fitting parameters for the three samples listed in Tables 1 and 2.

Table 1. Physical parameters for samples A, B, and C.

Sample	A	B	C
$P_O/10^{-7}$ mbar	75	26	6
n(300 K)/10^{17}cm^{-3}	2.3	21	69.7
E_d/meV	113	63.7	51.2
$N_d/10^{18}$ cm^{-3}	2.26	27.9	189.2
r_D/nm	8.55	3.70	1.96
$N_{Co}/10^{21}$ cm^{-3}	2.07	2.07	2.07
r_{Co}/nm	0.88	0.88	0.88

According to the non-degenerate single energy level donor semiconductor model,[26] we have the following relation in $Zn_{1-x}Co_xO$ films

$$n = \left(\frac{N_d N_C}{g_D}\right)^{1/2} \exp\left[-\frac{E_d}{2k_B T}\right], \quad (4)$$

where n is the carrier concentration, N_d is the donor density, N_C is the effective conduction band density of states, g_D=2 is the spin degeneracy for hydrogenic donor, and E_d is the activation energy. Here, $N_C = 2(2\pi m^* k_B T/h^2)^{3/2} = 3.72\times10^{18}$ cm^{-3} at 300 K, with h being the Planck's constant and $m^* = 0.28m_0$ being the effective mass of electron in ZnO (m_0 is the rest mass of free electron). The carrier concentration n is determined through the Hall effect measurement. All the samples show the n-type conduction. According to Eq. (4), donor density N_d can be obtained from the known n, N_C, and E_d. The average spaces between the donors, r_D, is calculated through a close packing face-centred cubic form: $r_D = 1/\sqrt{2} \times \sqrt[3]{4/N_d}$. Similarly, we can obtain the average spaces between Co^{2+} ions, $r_{Co} = 1/\sqrt{2} \times \sqrt[3]{4/N_{Co}}$, where N_{Co} is the concentration of Co^{2+} ions. All relevant parameters are listed in Table 1.

Table 2. Fitting parameters from Eqs. (2) and (3) for samples B and C.

Sample	ν_{ph}/cm^{-1}	T_M/K	α/nm^{-1}	ξ/nm	$N(E_{mF})$/cm^{-3}·eV^{-1}	R_M(5 K)/nm	R_M(300 K)/nm
B	1.7×10^{13}	2822.4	0.074	13.5	3.03×10^{19}	24.7	8.87
C	1.7×10^{13}	1480.5	0.103	9.74	1.53×10^{20}	15.2	5.45

The values of concentration of Co^{2+} ions N_{Co} in the three samples are the same (2.07×10^{21} cm^{-3}), but their values of donor density N_d are quite different (2.26×10^{18}, 27.9×10^{18}, 189.2×10^{18} cm^{-3} for samples A, B, and C, respectively). Therefore, N_d, rather than N_{Co}, is more important for the observed differences in VRH behaviours.

Anomalous Hall effect (AHE) is a useful tool to study the spin polarized current.[20] Figures 4(a)–4(c) show the curves of magnetic field (H) dependent anomalous Hall resistivity ρ_{xy}^{AHE} for samples A, B, and C, respectively. No AHE behaviour is observed for sample A. The AHE for sample B is noisy, which may be due to the large resistance and weak ferromagnetism. Obvious AHE is observed for sample C below 160 K as shown in Fig. 4(c). However, the ferromagnetism in sample C is maintained up to room temperature. It is noticed that the magnetic field-dependent ρ_{xy}^{AHE} does not match well with the M–H hysteresis curve for sample C. AHE shows an unsynchronous change with magnetism.

The ferromagnetisms for samples B and C can be explained with the bound magnetic polaron (BMP) model through local percolation.[12] Since the possible Cobalt oxide, such as Co_3O_4 and CoO, are not observed by XRD and RHEED, and furthermore both Co_3O_4 and CoO are antiferromagnetic at low temperature,[27,28] the extrinsic ferromagnetic origin of cobalt oxide can be excluded. Considering the powerful oxidbillity of radical oxygen and high crystal quality of the ZnCoO film, the possible existence of a Co cluster is also excluded. Oxygen vacancies are believed to be the effective donors for the room temperature ferromagnetism and AHE in the Co-doped ZnO magnetic semiconductor prepared under the oxygen-insufficient condition.[14–16,29,30] An oxygen vacancy can trap one electron, which couples with many Co^{2+} ions around to form a bound magnetic polaron. The radius of BMP sphere,[12] R_{BMP}, can be estimated by $R_{BMP} = \varepsilon(m_0/m^*)a_0 = 0.76$ nm, where $\varepsilon = 4$ for ZnO is the high frequency dielectric constant, and $a_0 = 0.053$ nm is Bohr radius. As shown in Table 1, the average space between oxygen vacancy donors, r_D, for each of the three samples is estimated. It is clear that the values of r_D are much larger than $2R_{BMP}$ for samples A and B and a little larger for sample C. If all defects are in a uniform distribution and if all BMPs are centred at these defects, the BMPs are far from ferromagnetic coupling. However, inhomogeneous distribution of defects can form local BMP-rich region, and some of the BMPs may overlap and/or be close to each other to form ferromagnetic coupling in it,[12,31]

especially for sample C. This is named local percolation, and many local ferromagnetic regions can be formed. The distances between these local ferromagnetic regions should have a similar scale to $r_{\rm D}$. The saturation magnetization of the Co^{2+} ions in sample C is rather smaller (0.22 $\mu_{\rm B}/Co^{2+}$) than that of metallic Cobalt. It means that only part of the Co^{2+} ions are in the ferromagnetic region. At the same time, with the number of donors increasing, the saturation magnetization of the Co^{2+} is enhanced. All the above results support the existence of a local ferromagnetic region, which contributes to the total ferromagnetism as indicated by SQUID and AGM measurements.

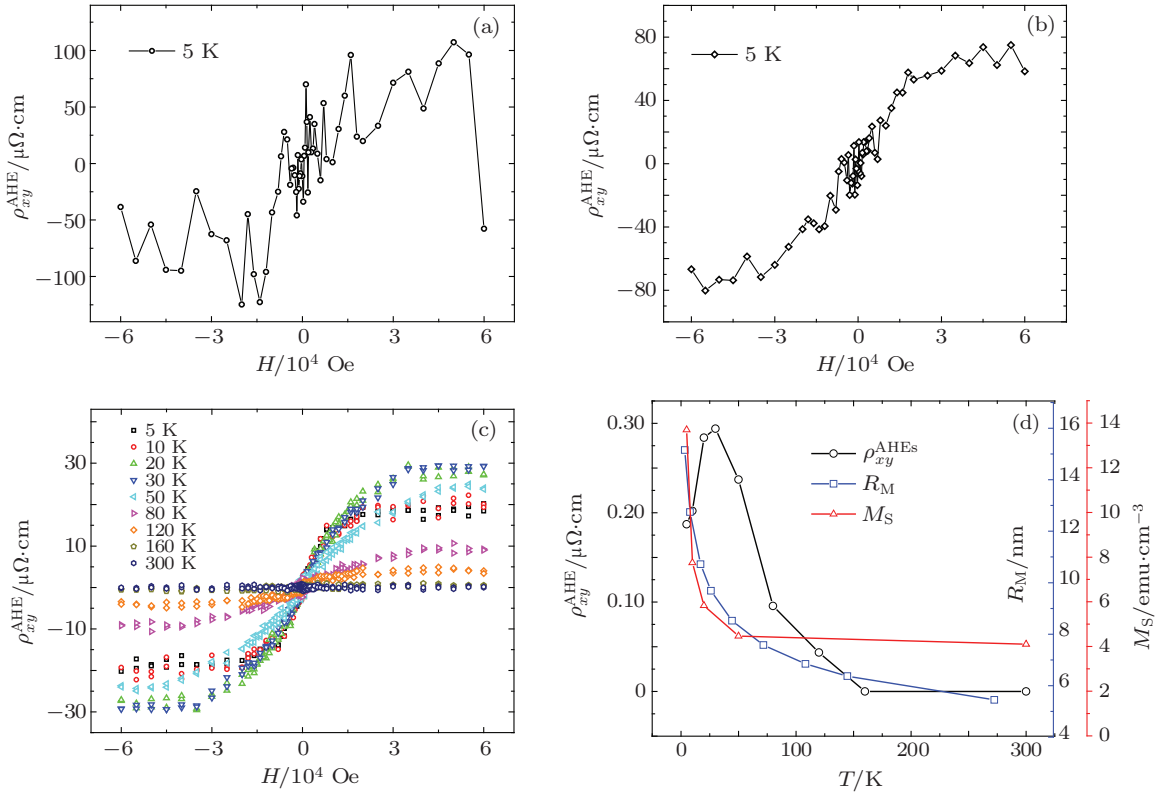


Fig. 4. (colour online) Magnetic field (H) dependent anomalous Hall resistivity $\rho_{yx}^{\rm AHE}$ curves for (a) sample A at 5 K, (b) sample B at 5K, and (c) sample C between 5 K and 300 K. Panel (d) shows temperature-dependent saturation anomalous Hall resistivity ($\rho_{xy}^{\rm AHEs}$), optimal hopping distance ($R_{\rm M}$) and saturation magnetization ($M_{\rm S}$) for sample C.

On the other hand, the charge transport in the Co-doped ZnO magnetic semiconductor is dominated by the phonon-assisted hopping of electrons trapped in the local donor states, such as oxygen vacancies, from the occupied states to the unoccupied states at low temperature. The temperature-dependent saturation anomalous Hall resistivity ($\rho_{xy}^{\rm AHEs}$), optimal hopping distance ($R_{\rm M}$), and saturation magnetization ($M_{\rm S}$) for sample C are shown in Fig. 4(d). The values of $M_{\rm S}$ and $\rho_{xy}^{\rm AHEs}$ are from Figs. 1(d) and 4(c), and the values of $R_{\rm M}$ are obtained from Eq. (3) respectively. Usually, the spin-polarized electrons can form in one isolated local ferromagnetic region from splitting bands or states[12] and AHE may appear in the small region. The transport of the spin-polarized electrons between different local ferromagnetic regions is affected by the ratio of the hopping distance to the distance between local ferromagnetic regions. From a macroscopic viewpoint, at low temperature the optimal hopping distance is large (about 15 nm at 5 K). In this case, the optimal hopping distance could be larger than the most of the distances between the nearest neighbouring local ferromagnetic regions. Then the spin-polarized electrons keep their spin polarization in the hopping process and the AHE can be observed. On the contrary, the optimal hopping distance decreases at high temperature, and it may be less than the distance between the nearest neighbouring local ferromagnetic regions. In this case, the spin memory may be lost in the hopping process and the AHE cannot be observed, although the local ferromagnetism still exists. According to this, in order to

obtain high spin-polarized current and AHE at higher temperature, the distance between local ferromagnetic regions should be reduced and higher doping levels of the donors and Co^{2+} ions are needed.

4. Conclusions

A series of high quality single crystalline epitaxial $Zn_{0.95}Co_{0.05}O$ thin films are prepared by molecular beam epitaxy. Superparamagnetism and ferromagnetism are observed when the donor density is manipulated in a range of 10^{18} cm^{-3}–10^{20} cm^{-3} by changing the oxygen partial pressure in growth. The conduction shows variable range hopping at low temperature and thermal activation conduction at high temperature. The ferromagnetism can be maintained up to room temperature, but the anomalous Hall effect appears at low temperature and disappears above 160 K. This phenomenon is explained on the basis of local ferromagnetism and the reduced optimal hopping distance at high temperatures.

References

[1] Pearton S, Norton D, Heo Y, Tien L, Ivill M, Li Y, Kang B, Ren F, Kelly J and Hebard A 2006 *J. Electron. Mater.* **35** 862

[2] Fu W Y, Cao J, Li Y X and Yang H B 2011 *Acta Phys. Sin.* **60** 067505 (in Chinese)

[3] Qiu D Q, Fan W Z, Weng S, Wu H Z and Wang J 2011 *Acta Phys. Sin.* **60** 087301 (in Chinese)

[4] Sati P, Schafer S, Morhain C, Deparis C and Stepanov A 2007 *Superlattices Microstruct.* **42** 191

[5] Xu Q Y, Zhou S, Marko D, Potzger K, Fassbender J, Vinnichenko M, Helm M, Hochmuth H, Lorenz M, Grundmann M and Schmidt H 2009 *J. Phys.* D: *Appl. Phys.* **42** 085001

[6] Ney A, Kammermeier T, Ollefs K, Ye S, Ney V, Kaspar T C, Chambers S A, Wilhelm F and Rogalev A 2010 *Phys. Rev.* B **81** 054420

[7] Alaria J, Bieber H, Colis S, Schmerber G and Dinia A 2006 *Appl. Phys. Lett.* **88** 112503

[8] Ye S, Ney V, Kammermeier T, Ollefs K, Zhou S, Schmidt H and Ney A 2010 *J. Phys.: Conf. Ser.* **200** 052034

[9] Li S S and Hu Y M 2011 *J. Phys.: Conf. Ser.* **266** 012018

[10] Gacic M, Jakob G, Herbort C, Adrian H, Tietze T, Brück S and Goering E 2007 *Phys. Rev.* B **75** 205206

[11] Jalbout A F, Chen H and Whittenburg S L 2002 *Appl. Phys. Lett.* **81** 2217

[12] Coey J M D, Venkatesan M and Fitzgerald C B 2005 *Nat. Mater.* **4** 173

[13] Behan A J, Mokhtari A, Blythe H J, Score D, Xu X H, Neal J R, Fox A M and Gehring G A 2008 *Phys. Rev. Lett.* **100** 047206

[14] Yan W, Jiang Q, Sun Z, Yao T, Hu F and Wei S 2010 *J. Appl. Phys.* **108** 013901

[15] Hu S J, Yan S S, Zhao M W, Lin X L, Yao X X, Han C, Tian Y F, Chen Y X, Liu G L and Mei L M 2011 *Scripta Mater.* **64** 864

[16] Liu E Z, Jiang J Z, Hsu H S, Lin C P, Chou H, Huang J C A and He Y 2010 *J. Appl. Phys.* **107** 023909

[17] Vidya R, Ravindran P, Fjellvág H, Svensson B G, Monakhov E, Ganchenkova M and Nieminen R M 2011 *Phys. Rev.* B **83** 045206

[18] Lajn A, von Wenckstern H, Benndorf G, Dietrich C P, Brandt M, Biehne G, Hochmuth H, Lorenz M and Grundmann M 2010 *Shallow Donors and Compensation in Homoepitaxial ZnO Thin Films* (Boston: Springer) p. 595

[19] Look D C, Farlow G C, Reunchan P, Limpijumnong S, Zhang S B and Nordlund K 2005 *Phys. Rev. Lett.* **95** 225502

[20] Hsu H S, Lin C P, Sun S J and Chou H 2010 *Appl. Phys. Lett.* **96** 242507

[21] Tiwari A, Jin C, Narayan J and Park M 2004 *J. Appl. Phys.* **96** 3827

[22] Tian Y F, Yan S S, Cao Q, Deng J X, Chen Y X, Liu G L, Mei L M and Qiang Y 2009 *Phys. Rev.* B **79** 115209

[23] Huang Y L, Chiu S P, Zhu Z X, Li Z Q and Lin J J 2010 *J. Appl. Phys.* **107** 063715

[24] Efros A L, van Nguyen L and Shklovskii B I 1979 *J. Phys.* C: *Solid State Phys.* **12** 1869

[25] Brodsky M H, ed. 1979 *Topics in Applied Physics: Amorphous Semiconductors* 36 (Berlin: Springer-Verlag) p. 127

[26] Ye L 2007 *Semiconductor Physics I* (Beijing: High Education Press) p. 191

[27] Roth W L 1964 *J. Phys. Chem. Solids* **25** 1

[28] Gielisse P J, Plendl J N, Mansur L C, Marshall R, Mitra S S, Mykolajewycz R and Smakula A 1965 *J. Appl. Phys.* **36** 2446

[29] Hanafin R and Sanvito S 2010 *J. Magn. Magn. Mater.* **322** 1209

[30] Xu Q, Hartmann L, Schmidt H, Hochmuth H, Lorenz M, Schmidt-Grund R, Sturm C, Spemann D and Grundmann M 2006 *Phys. Rev.* B **73** 205342

[31] Chou H, Lin C P, Huang J C A and Hsu H S 2008 *Phys. Rev.* B **77** 245210